Aluminium plasmonics

2015 J. Phys. D: Appl. Phys. 48 184001

(http://iopscience.iop.org/0022-3727/48/18/184001)

IOP Publishing Journal of Physics D: Applied Physics

J. Phys. D: Appl. Phys. **48** (2015) 184001 (14pp) doi:10.1088/0022-3727/48/18/184001

Aluminium plasmonics

Davy Gérard[1] **and Stephen K Gray**[2]

[1] Institut Charles Delaunay—LNIO, Université de Technologie de Troyes, UMR CNRS 6281, Troyes, France
[2] Center for Nanoscale Materials, Argonne National Laboratory, Argonne, IL 60439, USA

E-mail: davy.gerard@utt.fr and gray@anl.gov

Received 8 August 2014, revised 30 September 2014
Accepted for publication 2 October 2014
Published 15 December 2014

Abstract

We present an overview of 'aluminium plasmonics', i.e. the study of both fundamental and practical aspects of surface plasmon excitations in aluminium structures, in particular thin films and metal nanoparticles. After a brief introduction noting both some recent and historical contributions to aluminium plasmonics, we discuss the optical properties of aluminium and aluminium nanostructures and highlight a few selected studies in a host of areas ranging from fluorescence to data storage.

Keywords: surface plasmons, aluminium, nanostructures

(Some figures may appear in colour only in the online journal)

1. Introduction

Surface plasmons are coherent excitations of conduction electrons near the surfaces of metallic structures, i.e. near metal/dielectric interfaces [1–3]. They manifest themselves as evanescent electromagnetic surface waves and can be generated in a given system with appropriate external interactions with electrons or photons, for example. Surface plasmon polaritons (SPPs) are propagating surface plasmons in/on extended structures generally involving metal films or structured metal films. Localized surface plasmons (LSPs) are standing wave surface plasmons that are often excited on metal nanoparticle structures. While many of the basic ideas underlying surface plasmons go back many years, the field of study of surface plasmons, now known as 'plasmonics' [4], has only been rapidly growing since the early 1990s. This growth can be correlated with the general growth and interest in nanoscience and nanotechnology and has led to a great variety of plasmonic phenomena of both fundamental and practical relevance.

Most plasmonics work has involved the proposal and study of metallic nanostructures containing gold or silver. These noble metals exhibit plasmon resonances in the visible spectral region and have convenient properties. For example gold is relatively robust to oxidation. Silver, on the other hand, is less robust to oxidation but exhibits more narrow and intense LSP resonances. However, as plasmonics continues to expand, researchers are reaching out beyond such noble metals to other possibilities. The plasmonic response of aluminium nanostructures, in particular, is beginning to be significantly explored by many groups, e.g. [5–20].

One reason for the interest in aluminium plasmonics is that aluminium's plasma frequency is higher than that of gold or silver and this essentially allows for significant surface plasmon responses to occur in the ultraviolet (UV) portion of the spectrum, whereas gold and silver typically involve visible plasmons. This is relevant, for example, to applications of plasmonics ideas to the detection of organic and biological systems that exhibit strong UV absorptions and to photocatalysis. Furthermore aluminium, as we all know, is a relatively economical and manipulatable material, that opens up more avenues for fabrication and mass production. It is furthermore a very stable metal, due to the formation of a self-limiting native oxide layer protecting the metal surface from further oxidation and from contaminants. (The formation of this native oxide is discussed in greater detail in section 2.)

Actually, 'aluminium plasmonics' is perhaps not so new. Indeed, an argument can be made that the modern era of plasmonics began with the prediction, in 1957, by Ritchie of the possible existence of a peak in electron energy loss spectra (EELS) of thin metal films due to surface plasmons [21] and the first observation of such a peak being made by Powell and Swan in 1959 [22] using thin films of aluminium. Thus the study of aluminium plasmonics can be traced to the very birth of plasmonics over fifty years ago. Subsequent work on surface plasmons in aluminium films includes [23–26]. We also note that the first EELS observation of LSP resonances

on nanoparticles was performed on small aluminium nanoparticles [27].

In this introductory review for the special issue of the Journal of Physics D on aluminium plasmonics, we discuss the suitability of aluminium as a plasmonic material (section 2), the optical properties of several types of aluminium nanostructures (section 3) and several applications areas (section 4). Please note that the important topic of fabrication of aluminium nanostructures will not be discussed in this article, as it is the subject of a dedicated review in the same issue [28].

2. Aluminium as a plasmonic material

2.1. Optical properties and band structure

Aluminium is a very good metal exhibiting a high density of free electrons, with 3 electrons per atom in its conduction band (versus 1 electron/atom for gold and silver). The bulk plasmon frequency is directly related to this number as [1, 3]:

$$\omega_p = \sqrt{\frac{ne^2}{\varepsilon_0 m}} \tag{1}$$

where n is the density of free electrons, e the electric charge, m the effective mass and ε_0 the dielectric permittivity of vacuum. For aluminium, $\omega_p \approx 15$ eV. In comparison, $\omega_p \approx 8$–9 eV for gold and silver. In the simplest (Drude) model for a metal and considering a simple metal/air interface, surface plasmons are predicted to occur in the frequency range $0 \leqslant \omega \leqslant \omega_s$, where $\omega_s = \omega_p / \sqrt{2}$ is the quasi-static surface plasmon frequency. The relatively high value of ω_p indicates how broad is the frequency range where surface plasmons are allowed in aluminium.

The optical properties of aluminium can be understood by considering figure 1, showing the real and imaginary parts of the dielectric function of Al, taken from [29], for the UV, visible and near-infrared range. On figure 1 is also plotted the same set of data for gold and silver, for comparison. First, apart from the feature around $\lambda = 800$ nm (associated with the interband transition), aluminium exhibits a very 'Drude-like' (free electron) behaviour. Looking at the real part of the dielectric function (figure 1(a)), it appears that aluminium keeps a negative value of ε_1 (i.e. exhibits a metallic character) over a broader range than gold and silver. This is a direct consequence of the aforementioned value of ω_p. The imaginary part of ε (figure 1(b)) is directly related to losses inside the metal and the situation is less favourable to aluminium with respect to silver and gold. This is why gold and silver are the favoured metals for plasmonics: the imaginary parts of their dielectric functions are kept low over all the visible spectrum. However, due to the presence of interband transitions, gold and silver can not be used in the UV range, whilst aluminium exhibits both $\varepsilon_1 < 0$ and a relatively low ε_2 in the UV. This is why aluminium is such an appealing material for UV-plasmonics.

Another important feature is the fact that the interband transition (IT) in aluminium is a spectrally localized band around $\lambda = 800$ nm. For gold and silver, the IT is a threshold: all incident photons with wavelengths shorter than (roughly) 500 nm for gold and 310 nm for silver will predominantly excite electron-hole pairs. In gold this phenomenon stems from a transition between the d-like band and the sp-like band around the L symmetry point starting for energies higher than 2.4 eV [31]. This means that plasmon resonances can be observed only for wavelengths higher than the IT threshold. In contrast, aluminium can sustain surface plasmon resonances at wavelengths higher or shorter than the IT band. Further insight can be gained by considering the electronic band structure of aluminium (figure 2). Electrons close to the Fermi level can experience interband transitions near the W point (between the occupied p-like W'_2 state and the unoccupied s-like state W_1) and between the two parallel bands Σ_3 and Σ_1 [32]. The observed IT energy matches the energy gap between these bands, that is 1.5 eV (corresponding to $\lambda = 800$ nm). Interestingly, near the symmetry points W and K, the bands can be nicely approximated by a quadratic expression [32]. Hence, IT transitions in aluminium resemble closely transitions between the conduction and valence bands in direct gap semiconductors. Since the bands involved are parallel, photons with energies higher than the IT can not excite electron–hole pairs, explaining why the IT band is narrow.

2.2. The oxidation issue

Aluminium is sometimes argued to be unsuitable for plasmonics because it is known to oxidize rapidly, therefore leading to deteriorated optical properties. However this argument is an oversimplification. It is true that a native layer of alumina (Al_2O_3) appears on the surface of an Al particle or an Al layer in a matter of minutes when exposed to air. Langhammer *et al* used angle-resolved x-ray photoelectron spectroscopy (XPS) to study the oxidation of 20 nm thick aluminium films [7]. Measurements show that a native oxide layer is formed within a few hours of air exposure, with a thickness *stabilizing* at 2.5–3 nm (figure 3(a)). The oxide layer thickness then remains stable for at least 30 days, showing that the native oxide acts as a passivation layer preventing further oxidation. No bulk oxidation is therefore observed, in striking contrast to the oxidation of silver nanostructures, for instance.

Oxidation in aluminium nanoparticles (NPs) has been thoroughly studied by Knight and coworkers [17]. Using e-beam lithography, they made 100 nm diameter Al nanodisks with different oxidation fractions. The level of oxidation of the Al nanoparticles was controlled during the metal deposition by introducing small amounts of oxygen inside the deposition chamber. The scattering spectra of the Al NPs were then measured and are shown on figure 3(b). Starting from a resonance around $\lambda = 400$ nm for a pure Al NP (0% oxide), when the oxide fraction is increased the scattering efficiency decreases and the resonance maximum red shifts. When the oxide fraction reaches 50%, the plasmon resonance vanishes. Interestingly, the LSP linewidth does not dramatically increase in the process, meaning that the oxide fraction can be used as a parameter to tune the position of Al LSPs.

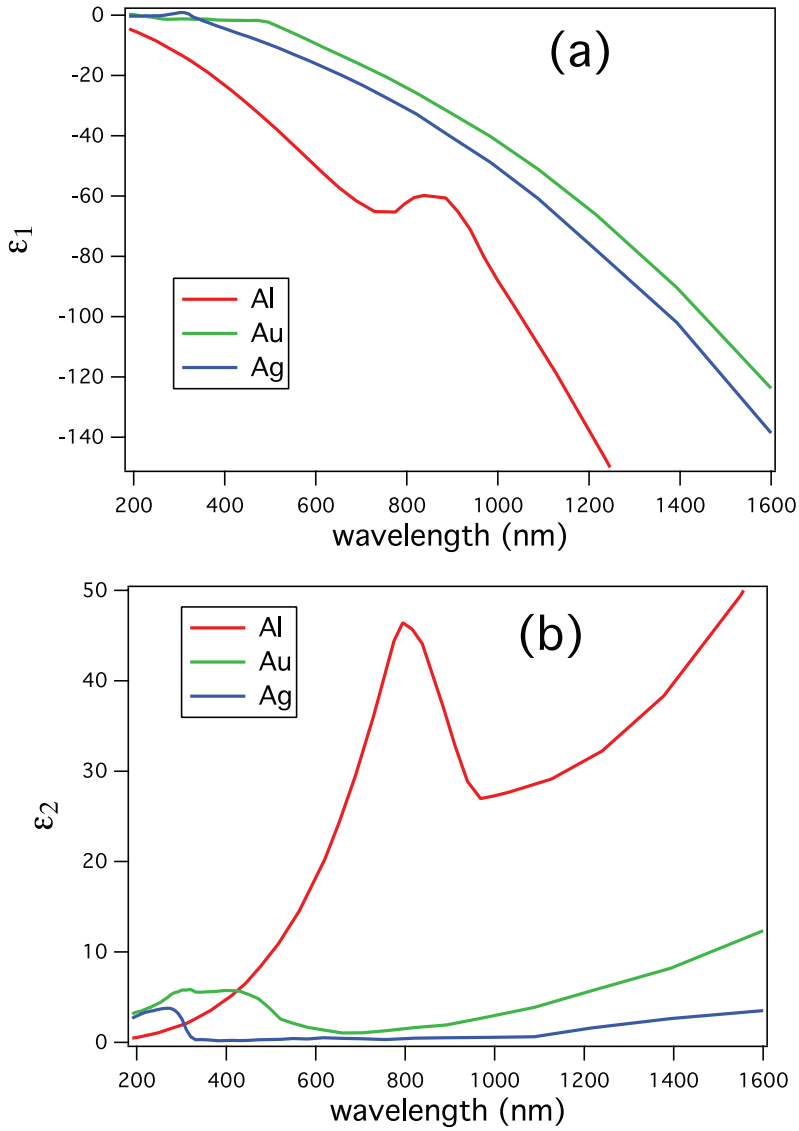

Figure 1. Real part (*a*) and imaginary part (*b*) of the dielectric functions for aluminium, gold and silver. Data from [29] (for Al) and [30] (for Au and Ag).

A more detailed study, including a phenomenological model for the formation of the oxide in Al nanoparticles, can be found in [33].

3. Optical properties of aluminium nanostructures

In this Section we review a few examples highlighting the plasmonic properties of aluminium nanostructures and thin films.

3.1. Surface plasmon polaritons in aluminium films

As noted in the Introduction, surface plasmon polaritons (SPPs) are propagating surface plasmon waves, generally propagating along some metal surface and evanescently decaying into both a dielectric superstrate (often simply air) and into the metal film. They can be characterized by a complex propagation vector with magnitude

$$k_{\mathrm{SPP}}(\omega) = \frac{\omega}{c}\sqrt{\frac{\epsilon_d \epsilon(\omega)}{\epsilon_d + \epsilon(\omega)}}\quad , \tag{2}$$

where ϵ_d is the dielectric constant of the superstrate and $\epsilon(\omega)$ is the metallic dielectric constant. The imaginary part of k_{SPP} is inversely proportionate to the propagation length, the latter being a general measure of the SPP quality for many applications. The nature of aluminium's dielectric constant is such that its SPPs are of particular high quality in the UV. Thus, for example, the focusing of aluminium SPPs has been visualized with photoresists sensitive to UV radiation [34] and there have been applications of aluminium SPPs in the detection of biomolecules that fluoresce in the UV [35] (see also section 4.1).

The focusing application noted above represents utilizing the fact that geometrical optics ideas can be used to understand SPP propagation. A recent theoretical study making use of such ideas developed a complex form of Snell's law

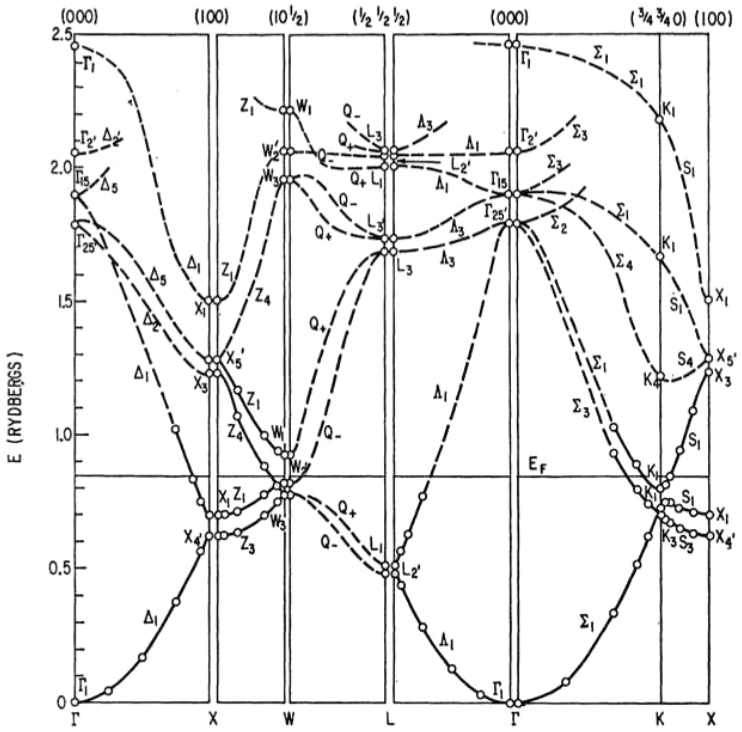

Figure 2. Calculated band structure of aluminium along the symmetry axes. Reprinted from [32]. Copyright 1963 American Physical Society.

and showed how SPPs on aluminium can be created via a refraction process and exhibit surprising dispersion relations [36].

3.2. Localized surface plasmon resonances in aluminium nanostructures

The optical responses (extinction spectra) of fabricated arrays of aluminium nanodisks with diameters ranging from ≈50 nm to 500 nm were studied by Langhammer *et al* [7]. This work showed how strong LSP resonances, with maxima tunable throughout the entire UV to visible to near-IR spectral regimes could be achieved with such aluminium nanoparticles. Thus, while aluminium enables achieving LSP resonances in the UV, one cannot discount its use (with appropriately large nanoparticle diameters) in the visible and near-IR. This work did, however, note a degradation of the nature of the aluminium LSP resonances near the 800 nm interband transition (section 2.1) and also discussed the nature of the oxidation of such particles (see also section 2.2). A related study was the work of Chan *et al* [6] on arrays of aluminium triangular nanoparticles fabricated via nanosphere lithography, which also affirmed many of the conclusions of [7]. A simple way of understanding the trends observed [6] is to examine the quasi-static (long wavelength) limiting expression for the extinction cross section, which can be written approximately as [6]

$$C_{\text{ext}} \propto \frac{1}{\lambda}\text{Im}\frac{\epsilon - \epsilon_{\text{med}}}{\epsilon + \chi\epsilon_{\text{med}}} \quad , \tag{3}$$

where $\epsilon = \epsilon(\omega)$ is the frequency (or equivalently wavelength) dependent dielectric function for aluminium discussed in section 2.1, ϵ_{med} is the medium dielectric constant and χ is a geometric factor that depends on the aspect ratio of the particle diameter to its height, with $\chi = 2$ being a sphere and ever larger values of χ occurring as this aspect ratio is increased (e.g. with diameter increasing for fixed height). While definitely not quantitative for all but the very smallest particle sizes, such a formula, coupled with the dielectric function of figure 1, helps to explain the trends observed in such experiments, including the red-shifts in LSP resonance with increasing aspect ratio. These authors also looked at the sensitivity of the extinction maxima to changes in refractive index (RI), i.e. RI sensing, and noted that increased oxidation at the sharp tips that can decrease this sensitivity.

More recently, the plasmonic properties of both aluminium nanorods [10] and nanodisks [17] have been examined by Knight *et al* These authors have envisioned that aluminium nanostructures could lead to a wealth of applications including, for example, high-area, low-cost CMOS-compatible, on-chip plasmonic nanoatennas, waveguides and interconnects. This work further affirmed the high tunability of LSP resonances—from the UV through to the visible part of the spectrum—that can be achieved with aluminium nanoparticles. This high tunability is illustrated in figure 4, where the scattering (dark-field) spectra of individual aluminium nanodisks with diameters ranging from 70 to 180 nm are shown. The nanodisk study [17], in particular, also examined in detail how the LSP resonances can shift in a predictable way as a function of the amount of oxide layer present (see figure 3(*b*)).

The scattering spectra from figure 4 also show that the smaller particle ($D = 70$ nm) exhibits a dipolar plasmon resonance around $\lambda = 300$ nm. With standard e-beam lithography

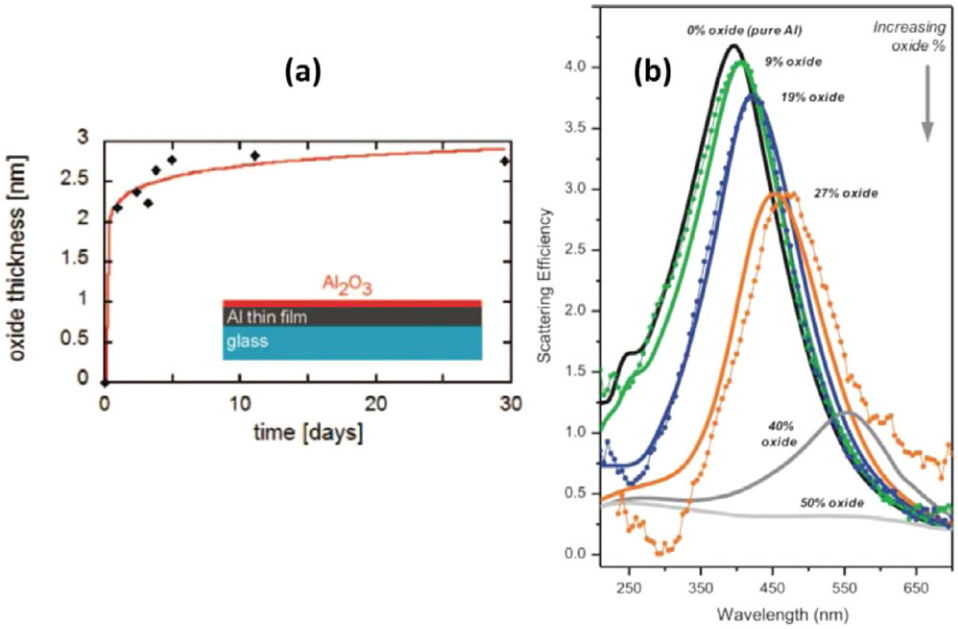

Figure 3. (*a*) Angle-resolved XPS measurements of the thickness of the native oxide layer onto a 20 nm thick Al layer. Marks are experimental data, the solid line is a direct logarithmic fit to the XPS data. Adapted with permission from [7]. Copyright 2008 American Chemical Society. (*b*) Scattering spectra of 100 nm diameter Al nanodisks with varying oxide fraction. Dotted lines correspond to experimental measurements, solid lines are FDTD calculations where the oxidation degree of Al is modelled with a Bruggeman effective medium. Adapted with permission from [17]. Copyright 2014 American Chemical Society.

techniques, it is difficult to reach particle sizes below 50–60 nm. This means that LSPs at deep UV wavelengths (below 300 nm) will be difficult to obtain with lithographed nanostructures. A first solution is to use other fabrication techniques to obtain small aluminium particles. For instance, Maidecchi *et al* using self-assembly techniques [11] and Martin *et al* using thermally annealed thin films [12] both obtained dipolar LSPs in the range 200–250 nm (see also the review by Martin and Plain in this issue for a glimpse of the wealth of techniques available to obtain small aluminium particles [28].).

It is also possible to obtain LSPs at deep-UV wavelengths without the need for very small nanoparticles by using higher-order LSP modes (i.e. quadrupole plasmon and higher modes). Going back to the scattering spectra from figure 4, the quadrupolar LSP appears as a high energy shoulder in the main dipolar resonance (higher order modes are also visible upon close inspection for the largest nanodisk structures). High order LSPs are generally weakly coupled to photons, explaining their relatively low scattering efficiencies. However, their intensity can be enhanced in some instances. Using dense aluminium NPs arrays, Jha *et al* observed an intense quadrupolar resonance around $\lambda = 250$ nm [37]. They were then able to use this resonance to enhance Raman signals (see section 4.2 for details on this application). The importance of higher order resonances for the scaling of LSPs toward deep-UV wavelengths was further underlined by Rodriguez *et al* in the case of Al 'nanocrescent' antennas [18]. Recently, the high-order LSP resonances sustained by Al nanorods (up to the $m = 4$ order) were experimentally observed and mapped in an electron microscope using EELS [20]. By analyzing the resonance linewidths, the authors observed that the quality factor of the resonances, for a given energy, increases with the resonance order.

3.3. Hybrid surface plasmon—interband modes

As presented in section 2.1, interband transitions (ITs) in aluminium appear as a narrow band around $\lambda = 800$ nm (1.5 eV). LSP resonances are allowed on both sides of the spectral band and when an LSP resonance approaches the IT a coupling phenomenon is observed. This coupling behaviour is reminiscent of the hybridation between LSP modes and has been predicted by Pakizeh [38]. The hybridation can be understood by considering a Drude-Lorentz model for the dielectric function of aluminium:

$$\begin{aligned}\varepsilon(\omega) &= \varepsilon_{\text{Drude}}(\omega) + \varepsilon_{\text{IT}}(\omega) \\ &= \left[1 - \frac{\omega_p^2}{\omega(\omega + i\gamma_c)}\right] + \left[\frac{G_0\omega_0^2}{\omega_0^2 - \omega^2 - i\Gamma\omega}\right] \end{aligned} \quad (4)$$

In this equation, the first term in square brackets is associated with the Al Drude-like behaviour, with γ_c the collision rate. The last term is a Lorentzian model of the IT, where ω_0 is the central frequency, G_0 is a gain and Γ the damping factor. If the dielectric function is fit with only the Drude contribution, one obtains a fictional metal resembling aluminium but without an IT. Equation (4) has been applied by Lecarme *et al* to Al nanoantennas [39]. Figure 5 displays the absorption and scattering cross-sections of 160×65 nm^2 Al nanorods, taking into account only the Drude part (dotted lines) and with the complete dielectric function (solid lines). For such a size, the dipolar Drude-LSP resonance would appear almost exactly at the IT frequency (dotted line in figure 5). However, the presence of the IT at the same frequency induces a split in both the absorption and scattering peaks (solid lines), with the appearance of two hybridized modes. In the case

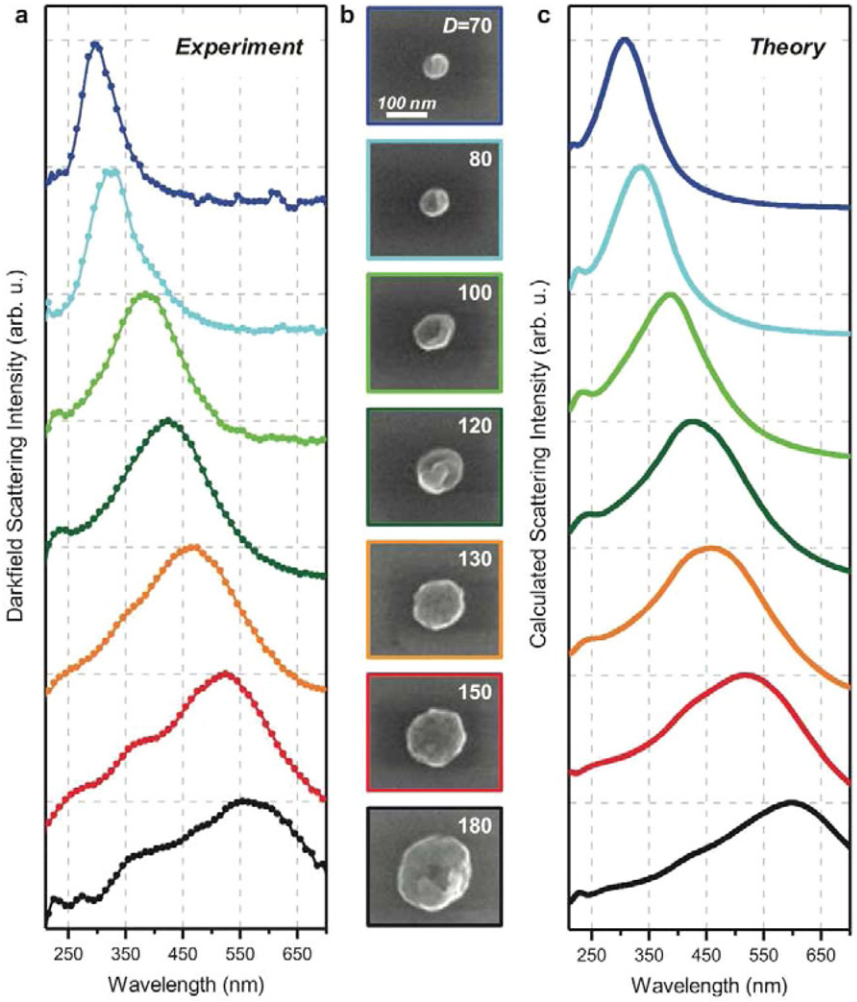

Figure 4. Tuning of the LSP resonance of Al nanodisks fabricated using e-beam lithography. (*a*) Experimental scattering spectra of individual nanodisks with varying diameters (D = 70, 80, 100, 120, 130, 150, 180 nm). (*b*) SEM images of the corresponding nanodisk structures. Scale bar is 100 nm. (*c*) Finite-difference time-domain (FDTD) simulations of the scattering spectra, assuming a 3 nm surface oxide and a SiO_2 substrate. Reprinted with permission from [17]. Copyright 2014 American Chemical Society.

of scattering, the scattering efficiency now shows a dip at the IT frequency. This behaviour is highly reminiscent of strong coupling between two oscillators: one oscillator being the surface plasmon, the other the IT. This strong coupling behaviour has been experimentally observed by Schwind and co-workers in an aluminium film perforated with holes [40]. The interaction between the LSP resonance and the IT was observed as anti-crossing when the LSP resonance frequency converges into the IT and vice-versa. This is a nice experimental verification of Pakizeh's prediction [38] in the case of Al. Thus, aluminium is an ideal material to observe the LSP-IT hybridation because of its spectrally narrow IT, behaving much like a dipole.

3.4. Non-linear optical properties

Non-linear optical properties of materials play an important role in photonics, enabling key applications such as ultrafast optical switching and all-optical signal processing. Plasmonics is no exception and non-linear plasmonics appears as an important topic (see [41] for a review). Remarkably, aluminium seems to exhibit very good non-linear optical properties when compared with other plasmonic metals [42–44].

The second-order non-linear optical susceptibility $\chi^{(2)}$ of aluminium thin films has been measured by Krause, Teplin and Rogers, using a Ti-sapphire laser operating at a central wavelength of 810 nm with a 50 fs pulse duration [42]. The bulk susceptibility of Al was found to be about one order of magnitude higher than that of gold and silver. However, the measured second harmonic generation (SHG) signal is higher for silver films than for aluminium films. The authors explain this apparent discrepancy by the fact the fundamental pumping wavelength falls into the aluminium IT, yielding a deteriorated transmission factor of the pump through the Al film.

The case of Al nanostructures might however be different, as second- and third-order non-linear susceptibilities are dominated by symmetry-breaking surface effects. A detailed study on the impact of geometry on the nonlinear response was reported by Castro-Lopez *et al* [43]. They analyzed both SHG (a second-order effect) and two-photon photoluminescence (TPPL, a third-order effect) arising from gold and aluminium

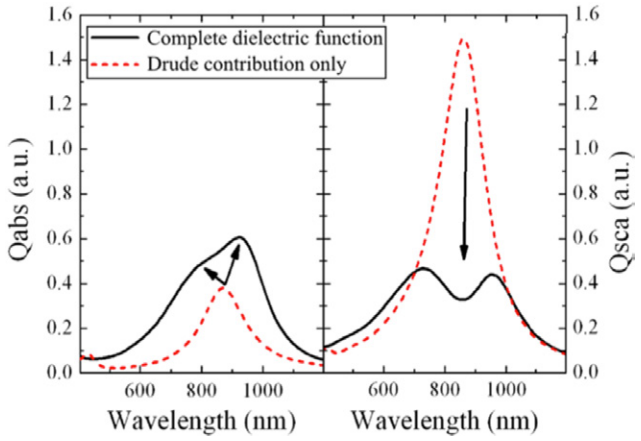

Figure 5. Calculated absorption cross-section (left panel) and scattering cross-section (right panel) of Al nanorods, using equation (4). Adapted with permission from [39]. Copyright 2014 American Chemical Society.

nanorods when excited with femtosecond pulses centred around $\lambda = 780$ nm. They observed strong SHG and TPPL signals from the Al nanorods when the rod length was resonant with the incident laser pulse. From their measurements and electromagnetic simulations, Castro-Lopez *et al* estimate that the nanorods' two-photon luminescence efficiency is two orders of magnitude higher in Al than in Au and Ag. However, the claim for strong SHG in Al nanoantennas has been recently contested, as Schwab *et al* measured the same SHG level in the presence and in the absence of Al nanoantennas [45]. They suggest that this signal is likely to come from the conductive oxide (ITO, indium tin oxide) covering the substrate. Hence, further research is requested to settle this issue and discriminate between the non-linear signal arising from the substrate and the one arising from the nanoparticule itself.

Third-harmonic generation (THG) in Al nanostructures was studied by Melentiev *et al* in [44]. Using excitation around $\lambda = 1500$ nm (thus outside the IT), they observed THG in aluminium films, nanoholes and nanoslits. The choice of nano-apertures rather than nanoparticles, which are complementary structures according to Babinet's principle, allows use of much higher excitation power without risking the destruction of the nanostructure under the incident laser flux. Based on thin film measurements, Melentiev *et al* estimate the $\chi^{(3)}$ coefficient of Al at $\lambda = 1500$ nm to be about 3 orders of magnitude higher than that of gold: $\chi^{(3)}_{\mathrm{Al}} = (2.6 \pm 0.8) \times 10^{-17}$ m^2 V^{-2}, whilst $\chi^{(3)}_{\mathrm{Au}} = (2.3 \pm 0.7) \times 10^{-20}$ m^2 V^{-2}. The same authors also reported that the THG response of Al could be made even higher by using C-shaped nano-apertures [46].

4. Applications

4.1. Fluorescence

The coupling of plasmons to fluorescing molecules, or fluorophores, is an important and active area of plasmonics reasearch with relevance to biological research and medical diagnostics. [47–51] In particular we should note the pioneering efforts of Lakowicz and co-workers on a myriad aspects of plasmon or metal enhanced fluoresence (MEF) and related phenomena such as surface plasmon coupled emission (SPCE) [47, 52]. Aluminium nanostructures, which can support plasmons in the UV spectral regime, are particularly important because many important biomolecules fluoresce in the UV.

Regarding MEF, the emission rate of a fluorescent dye in the vicinity of a plasmonic nanostructure can be modified (hopefully increased) by three different effects: (i) the local excitation field can be increased by the plasmonic resonance (*excitation enhancement*); (ii) the emission rate can be accelerated via the Purcell effect (*emission enhancement*) and (iii) fluorescence emission can be redirected more efficiently towards the detector (*antenna effect*) [3]. The three effects are generally interwoven.

A six-fold enhancement of fluorescence from Rhodamine-6G molecules inside sub-wavelength apertures milled in an opaque aluminium film was reported by Rigneault *et al* in 2005 [53]. The effect is attributed to field enhancement inside the aperture and not necessarily to surface plasmon excitation. Later, experiments performed at a wavelength of 633 nm showed that apertures milled in gold films outperform apertures in aluminium [54]. Again, the effect is linked to the existence of (evanescent) guided modes inside the nanoaperture. Similar experiments have been reported using bowtie nanoapertures milled in aluminium, sustaining propagating modes inside the apertures [55]. In the UV range, computations performed by Mahdavi and Blair [56] demonstrated that nanoapertures in Al would significantly enhance the emission of dyes under 266 nm excitation wavelength. Lakowicz and co-workers have also explored how aluminium nanostructured films can significantly enhance DNA base analogues [5] and serve as substrates for the label-free detection of amino acids [8].

UV-excitation is particularly interesting because most substances exhibit native fluorescence (or autofluorescence) under UV excitation. Most biomolecules absorb light in the range 220–280 nm. Label-free detection of biomolecules is thus possible using UV excitation, but is hindered by the low efficiency of native fluorescence. The design of plasmonic nanostructures resonating in the UV is hence a topic of interest for a number of biotechnological applications (e.g. label free detection, sensing and measurement of molecular kinetics) Jiao and Blair [57] proposed and numerically optimized three different antennas for fluorescence enhancement in the UV: dipole antennas (or gap antennas), Bull's eye structures and aperture arrays. Their study yields realistic parameters for an experimental realization, with predicted net enhancements factors of two orders of magnitude. In a simpler fashion, Ono *et al* [58] used an aluminium thin film illuminated in Kretschmann geometry and covered with quantum dots. Significant enhancement of the quantum dot fluorescence is observed when the 266 nm excitation is p-polarized and the angle set to the Kretschmann angle. The fluorescence enhancement is attributed to the high field enhancement ($\sim$ 40 times) on the Al film surface. Finally, we note that a detailed study of the interaction between an aluminium nanoparticle and a single emitting dipole was recently reported by Forestiere, Handin and Dal Negro [59].

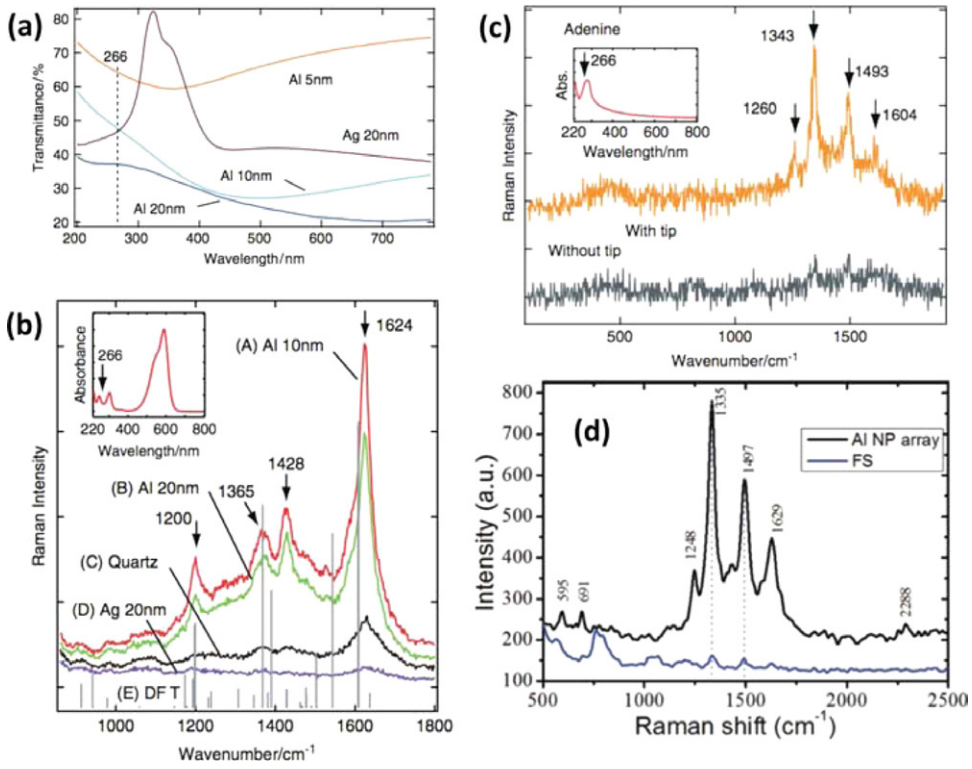

Figure 6. Surface-enhanced Raman scattering with aluminium films and nanoparticles. (*a*) Transmission spectra of evaporated Al and Ag films with various thicknesses. (*b*) Resonance Raman spectra of 30 μM crystal violet aqueous solution deposited on evaporated metal films: 10 nm thick Al film (red line), 20 nm thick Al film (green line), 20 nm thick silver film (violet line) and a reference quartz substrate (black line). The grey lines correspond to a density functional theory (DFT) calculation of the vibrational lines of crystal violet. Excitation laser wavelength 266 nm; excitation power 350 μW; acquisition time 300 s. Inset: UV-vis absorption spectrum of the crystal violet aqueous solution. (*c*) Deep-UV TERRS spectra of solid adenine nanocrystals. Excitation wavelength 266 nm; excitation power 180 μW; acquisition time 60 s. Inset: absorption spectrum of adenine nanocrystals. Adapted with permission from [61]. Copyright 2009 John Wiley and Sons. (*d*) Raman spectra of a 1 nm thick adenine film deposited either on a fused silica substrate (black line) or an array of Al nanodisk with 140 nm diameter. Excitation wavelength 257.2 nm; collection time 1 s. Adapted with permission from [37]. Copyright 2012 American Chemical Society.

SPCE involves fluorophores coupling into propagating surface plasmon polaritons (SPPs) on thin films [48, 50]; the directional emission from such SPPs represents a sensitive analytical tool for detecting fluorophores. Lakowicz and co-workers have shown how thin aluminium films can yield ultra-violet SPCE of UV-absorbing fluorophores, again pointing to the important practical applications of aluminium plasmonics in biological and medical research [35].

4.2. Surface enhanced Raman scattering

Surface enhanced Raman scattering (SERS) has been a leading applications area of plasmonics since the 1970s. SERS takes advantage of the intense and localized electromagnetic fields near metal nanostructures to enhance the otherwise weak process of Raman scattering. First discovered with thin films with surface roughness, SERS is now moving to more reproducible systems made with size-controlled nanostructures [60]. As the Raman scattering cross-section increases with the fourth power of the frequency, translating SERS into the deep-UV region might be interesting—if side issues, notably the autofluorescence of most materials in the UV region, can be avoided.

A first attempt was reported by Dörfer, Schmitt and Popp in 2007 [62]. They observed SERS with a crystal violet solution deposited on 50 nm thick Al film illuminated at $\lambda = 244$ nm. The SERS activity of aluminium was further confirmed by Taguchi *et al* [61] using thin Al films evaporated onto a quartz substrate. Their corresponding transmission spectra are plotted figure 6(*a*) (along with a reference sample consisting of a 20 nm thick silver film). Figure 6(*b*) shows the Raman spectra of a crystal violet solution measured on those samples for $\lambda = 266$ nm excitation, corresponding to a resonant excitation (see the crystal violet absorption spectrum in the inset of figure 6(*b*)). Surface-enhanced resonant-Raman scattering (SERRS) is clearly evidenced on this figure, with 10 nm thick Al film giving the best results. Interestingly, silver yields the poorest results, acting as an absorbing dielectric. In contrast to the previous study [62], Taguchi *et al* did not observe a significant spectral shift between the Raman lines measured on the SERS substrate and the normal Raman spectrum. Moreover, Taguchi *et al* performed tip-enhanced Raman scattering (TERS) by covering the surface of an atomic force microscope probe with a 25 nm thick Al layer. In TERS, the plasmonic enhancement is obtained below the tip apex, allowing one to spatially localize the molecules under study. On figure 6(*c*) is plotted a tip-enhanced resonant-Raman scattering (TERRS) spectrum of solid adenine. The TERRS effect is clearly demonstrated as the Raman lines at 1260, 1343, 1493 and 1604 cm^{-1} disappears when the tip is retracted from the surface.

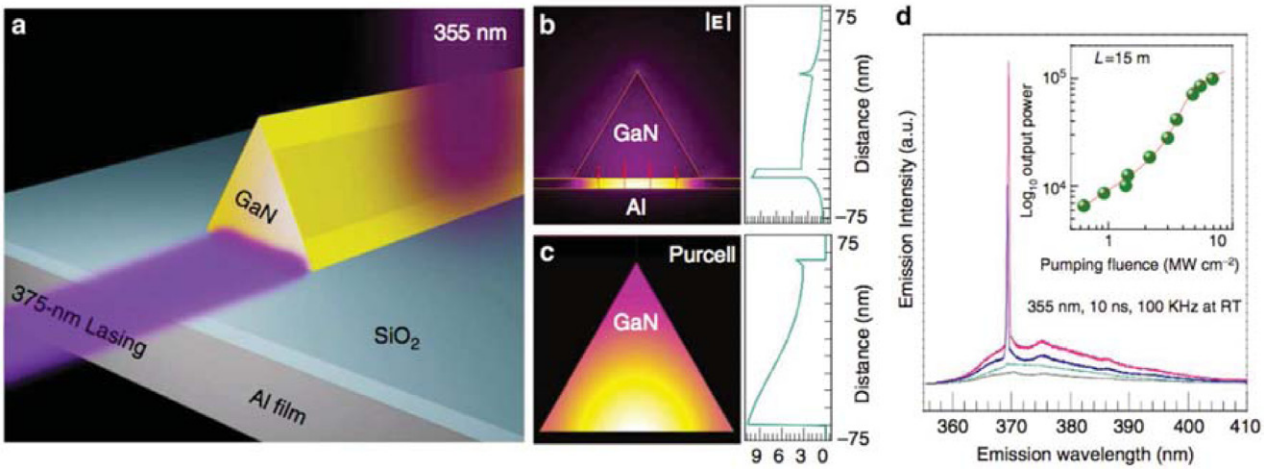

Figure 7. Ultraviolet plasmonic nanolaser. (*a*) Schematic of the structure. (*b*) Finite-element method calculation of the absolute electric field $|\mathbf{E}|$ around the device at $\lambda = 370$ nm, showing the high degree of energy confinement inside the insulator layer. Red arrows indicates the electric field direction. (*c*) Calculated Purcell factor distribution inside the GaN nanowire. (*d*) Experimental characterization of the laser emission: power-dependent emission spectra of the device, showing the appearance of a sharp peak above the spontaneous emission background. Inset: integrated emission as a function of the pumping intensity. Reprinted with permission from [66], Copyright 2014 Macmillan Publishers Ltd.

The use of shape- and size-controlled Al nanostructures for SERS was demonstrated by Jha *et al* [37]. Using extreme-UV interference lithography, they made arrays of Al nanodisks (with diameters in the range 65–140 nm) over a relatively large area (400 × 400 μm^2). A representative spectrum of a 1 nm thick adenine film measured on a fused silica substrate (blue line) and on a Al nanodisk array (black line) is shown in figure 6(*d*), evidencing the SERS effect. The authors estimate that their system is able to detect about 50 zeptomoles of adenine molecules (i.e. ∼ 30 000 molecules). It is worth noticing that as the laser excitation is located deep in the UV ($\lambda = 257.2$ nm). In this study the SERS effect stems from the field enhancement associated with the quadrupole LSP. Using extinction spectroscopy, Jha *et al* showed that the dipole plasmon of the nanodisk arrays is in the range 320–400 nm (depending on disk diameter), while the quadrupole LSP is around 250 nm, close to the laser excitation [37]. This is a nice illustration of the use of higher-order plasmon resonances for practical applications.

Recently, the SERS activity in the visible and near-infrared of a discontinuous Al thin film made by evaporation and thermal annealing has been discussed by Mogensen *et al* [63]. They observed a significant SERS signal for an excitation at $\lambda = 785$ nm, a wavelength where the extinction spectrum revealed no surface plasmon resonance and quite close from the interband transition. The authors correlate this near-infrared SERS activity with plasmon resonances in the 1.3–2.5 eV range measured using electron energy loss spectroscopy.

4.3. Optoelectronics

The ability of aluminium nanostructures to sustain surface plasmon resonances in the UV region of the spectrum is especially attractive for optoelectronics applications involving wide bandgap semiconductors. The band-edge emission of ZnO and GaN, for instance, is located around 3.35 eV (i.e. $\lambda = 370$ nm), out of reach of classical plasmonic materials. One of the first attempts to apply the plasmonic properties of aluminium to such optoelectronic devices was reported by Okamoto *et al* in 2004 [64]. They studied the emission from a layer of InGaN quantum wells inside a GaN layer coupled to an unstructured metal film made of gold, silver or aluminium. They observed a significant photoluminescence enhancement for Ag and Al, with Ag slightly outperforming Al. However, in this case the InGaN quantum well emission was in the blue region (around 470 nm), explaining the higher performance of silver. Using a similar approach, Gao and coworkers [65] reported plasmon enhanced deep-UV emission in AlGaN multi-quantum wells light emitting diodes. Thanks to a thin aluminium layer deposited onto the top of the structure, a 217% photoluminescence enhancement was observed at $\lambda = 294$ nm. This enhancement is attributed to a higher light extraction efficiency induced by the surface plasmon transverse magnetic wave coupling. This enhancement is wavelength dependent, the plasmon-enhanced light extraction being more efficient at shorter wavelengths.

Very recently, a plasmonic nanolaser emitting in the UV was demonstrated by Zhang and co-workers [66]. Their design is based on the 'deep-subwavelength scale plasmon laser' geometry that was previously devised for nanolasers emitting in the blue-green region [67]. Here, the gain medium is a triangular GaN nanowire, which is separated from an aluminium film by an ultra-thin (∼ 8 nm) layer of SiO_2 (figure 7(*a*)). The resulting Al/SiO_2/GaN structure sustains an hybrid plasmonic mode, whose electric field distribution is shown in figure 7(*b*). The electromagnetic energy appears to be highly concentrated inside the insulator layer, forming the laser cavity. Figure 7(*c*) shows the calculation of the associated Purcell factor distribution, showing that most of the GaN nanowire experiences a Purcell factor in the range 7–10. Under optical pumping with

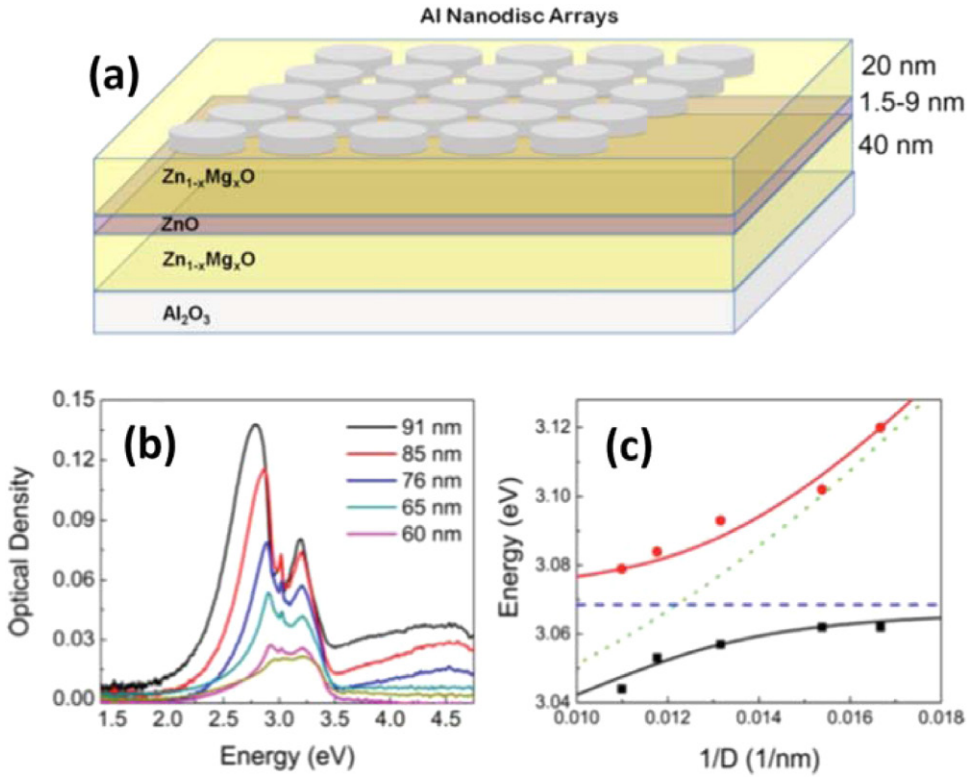

Figure 8. Coupling between Al nanodisks and a ZnO heterostructure. (*a*) Schematic of the structure. (*b*) Absorption spectra recorded at low temperature ($T = 77$ K) from the structure for different disk diameters. (*c*) Dispersion curve of the minima observed in the absorbance spectra (marks) superimposed with a coupled oscillators model (solid lines). The dashed blue line is the (uncoupled) exciton energy, the dashed green line depicts the quadrupole resonance as computed with Mie theory. Adapted with permission from [68]. Copyright 2012 American Chemical Society.

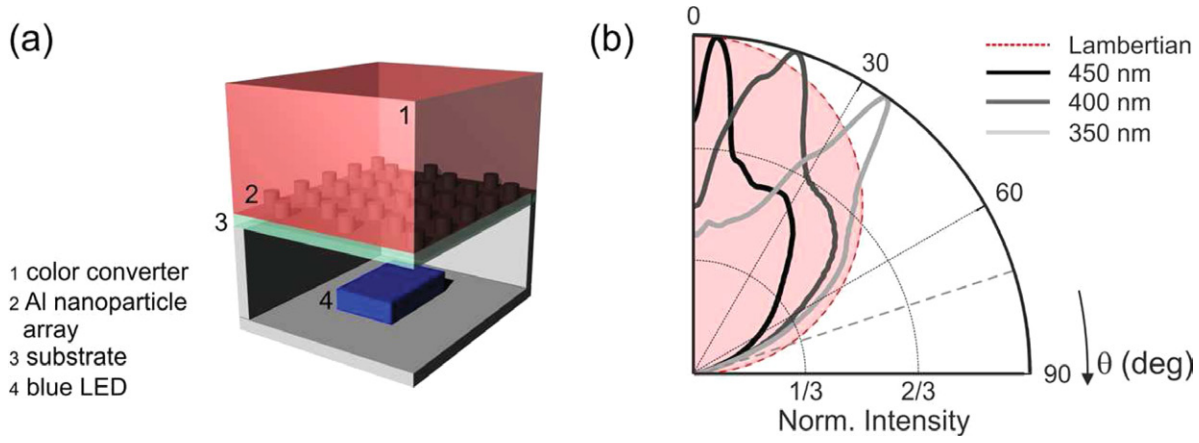

Figure 9. Directional emission from a light-emitting device due to aluminium nanoparticles. (*a*) Schematic of the structure: a photoconversion layer sits onto an array of Al NPs. The structure is illuminated with a blue light-emitting diode (LED). (*b*) Radiation pattern of the emitted luminescence measured by Fourier microscopy for three different values of the pitch of the array (solid lines). Lambertian emission is plotted for reference (red dotted line). Figure courtesy of Gabriel Lozano.

a 355 nm pulsed laser source, room-temperature laser emission at $\lambda \approx 370$ nm is observed in emission spectrum (figure 7(*d*)) as a sharp peak.

The effect of Al nanostructures on the emission from either bulk ZnO or ZnO heterostructures was reported in a couple of studies [68, 69]. Lawrie and co-workers [68] reported strong-coupling between ZnO quantum well excitons and Al nanoparticles surface plasmons. They deposited an array of Al nanodisks with variable diameter onto a heterostructure including a single ZnO/$Zn_{0.85}Mg_{0.15}O$ quantum well (figure 8(*a*)). The absorption spectra of the different structures were measured at low temperature—where the exciton binding energy and thus its oscillator strength, is high. Absorption dips are clearly visible in figure 8(*b*). These dips stem from strong coupling between the two oscillators (plasmon and exciton), resulting in the formation of an hybrid plasmon-exciton state. This behaviour is further confirmed by plotting the energy position of these dips as a function of the disk diameter (figure

8(*c*)). An anti-crossing (Rabi splitting) is clearly visible, with a corresponding coupling energy of 15 meV. This study is the first demonstration of exciton-plasmon hybridization in the near-UV range.

The effect of gold, silver and aluminium nanoparticles arrays on the detected photocurrent from GaAs photodiodes was studied by Hylton *et al* [14]. They observed a 22% increase of the integrated external quantum efficiency for a photodiode with Al NPs compared with a bare photodiode. In this case, Al clearly outperforms gold and silver since the photodiode maximum efficiency is in the blue-green range. A very similar result was previously obtained by Villesen *et al* for silicon photodiodes. In [70], they compared the performances of Al and Ag nanoparticles arrays to enhance the detected photocurrent. While Ag outperforms Al for wavelengths ranging from 570 nm to 1200 nm, on the whole spectrum (300 nm to 1200 nm) Al is better—exhibiting a 2.8% gain in the integrated photocurrent, compared to 1.2% for Ag. This further underlines the broadband plasmonic behavior of Al with respect to coinage metals. Using a different approach, the Halas group [71] recently proposed an Al-Si plasmonic photodetector based on a metal-semiconductor-metal geometry. In their design, the aluminium is involved in the Schottky junction (Al-Si junction) and an aluminium grating acts as a plasmonic color filter, sorting colors and providing an additional photocurent due to local field enhancement.

The efficiency of silicon solar cells is hindered in the UV and near-IR ranges by the optical properties of bulk silicon. Spectral conversion is a way to circumvent this issue by converting the UV (or near-IR) photons into visible photons—a process known as downshifting (and upshifting, respectively). The efficiency of those spectral conversion processes is however rather weak, limiting their use for practical applications. Plasmonic nanostructures have been suggested as a possible solution to increase the spectral conversion efficiency [72, 73]. Mupparapu and co-workers used Al nanoparticles to increase the efficiency of downshitfing of UV light [74]. Rather than relying on the increased emission or absorption in the vicinity of the nanoparticles (which requires a relatively high density of nanoparticles), they exploited the enhanced light scattering introduced by the Al nanoparticles. Al nanoparticles were diluted in a photoconversion layer containing a dye molecule absorbing in the UV and they observed an increased light absorption. This effect is explained by considering that an incident UV photon will be scattered by the nanoparticles, increasing its mean free path and hence its probability of absorption by the dye molecule. This approach is of interest because it uses only a relatively small amount of metallic nanoparticles, resulting in a transparent conversion layer in the visible range.

Colour-conversion layers are also used in solid-state lighting to obtain white light from a blue or UV source. Lozano and co-workers used aluminium plasmonics to enhance the efficiency of those conversion layers [16, 75]. In [75], they used a hexagonal array of Al nanoparticles to enhance and tailor photoconversion in a light-emitting device. A schematic of the structure is shown in figure 9(*a*). The Al NP array was obtained using nanoimprinting, allowing large-area nanopatterning of the conversion layer. The Al NP array not only increases the amount of detected light thanks to an enhanced light extraction efficiency, but also allows control of the radiation pattern of the photoconverted light. The enhanced directionality was evidenced using Fourier microscopy. Figure 9(*b*) shows that the emission angle can be tuned by varying the pitch of the array: the emission angle increases when the pitch decreases.

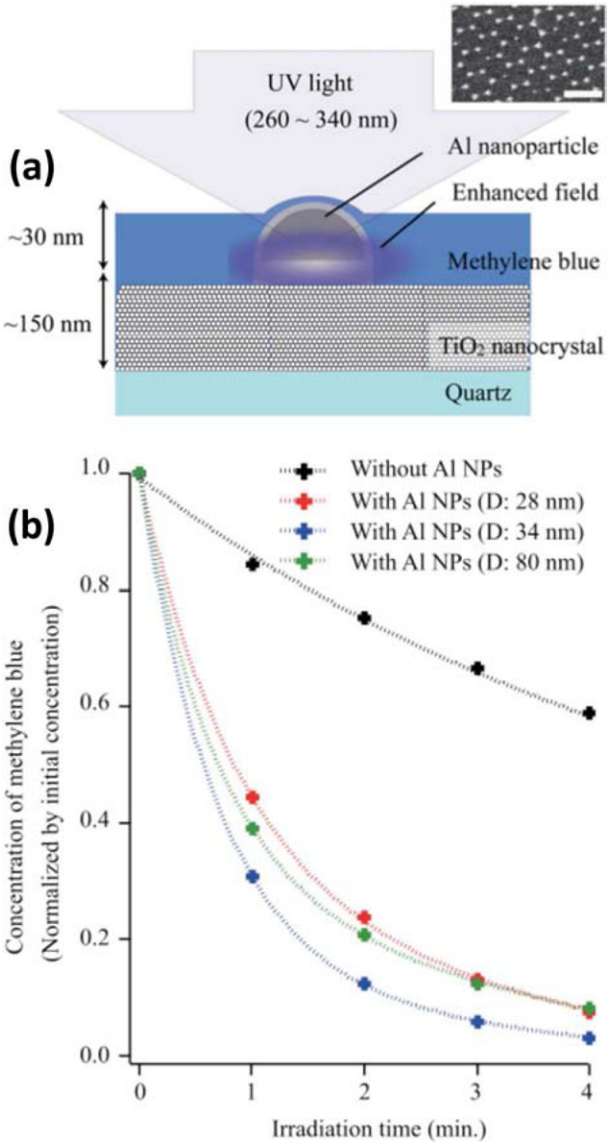

Figure 10. Plasmon-enhanced UV photocatalysis. (*a*) Schematic of the structure to study plasmon-enhanced photocatalysis of methylene blue degradation by TiO_2. (*b*) Kinetics of the photocatalytic reaction: methylene blue concentration versus irradiation time for different Al nanoparticle diameters. Reprinted with permission from [82]. Copyright 2014 AIP Publishing LLC.

4.4. Photocatalysis

Photocatalysis is another promising application field for aluminium plasmonics. A photocatalyst is a semiconductor or oxide (like TiO_2 or ZnO) that absorbs photons to

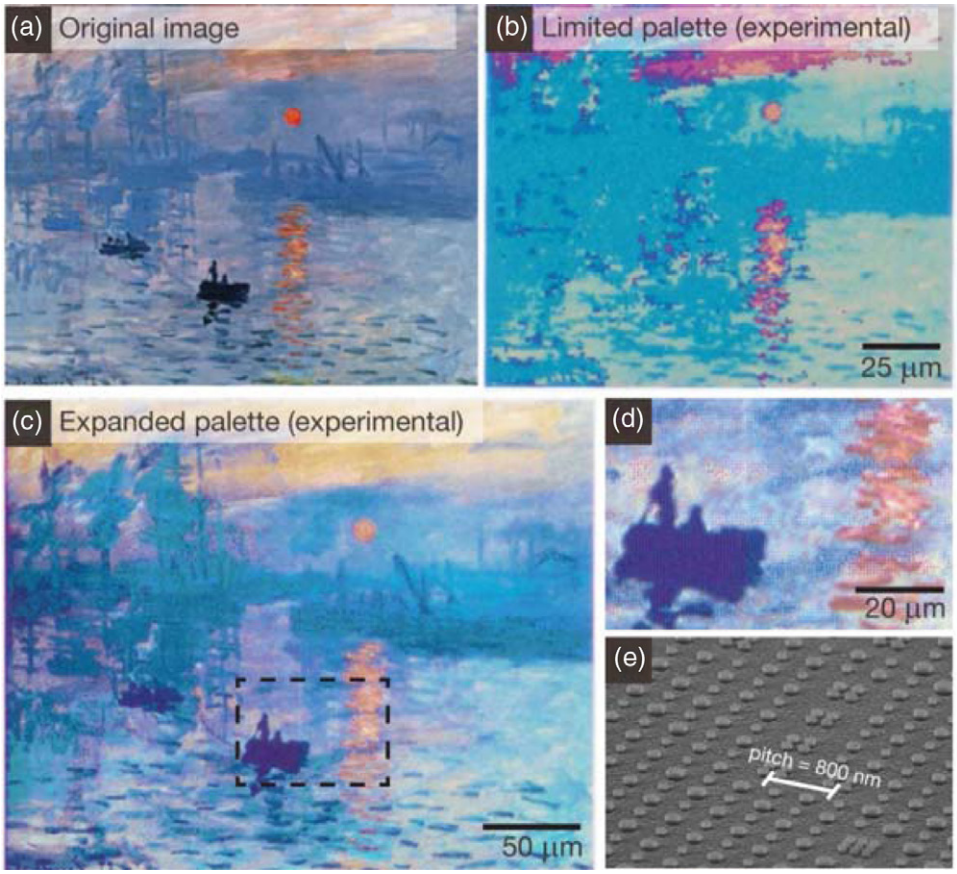

Figure 11. Structural colours from Al nanoparticles reproduce Monet's *Impression, soleil levant*. (*a*) Original image. (*b*) Reproduction using the 'limited plasmonic palette' (variation of the nanoparticles diameter). (*c*) Reproduction using the 'extented plasmonic palette' (variation of the nanoparticles diameter and spacing). (*d*) Higher magnification image of the previous panel. (*e*) SEM image of the plasmonic pixels. Reprinted with permission from [83]. Copyright 2014 American Chemical Society.

generate electron-holes pairs, which in turn generate free radicals. Subsequently, chemical reactions are induced at the surface of the photocatalyst [76]. For instance, the strong oxidizing power of TiO_2 has been used in many environment-related applications like air and water cleaning, disinfection and self-cleaning surfaces [77–79]. Plasmonic nanostructures have been demonstrated to enhance photocatalytic activity [80, 81].

As the energy of the incident photon should be higher than the bandgap energy in order to generate the electron-hole pair, UV light is generally involved. This is where Al nanostructures can help. Honda *et al* [82] demonstrated enhanced photocatalysis of methylene blue degradation by TiO_2 using Al nanoparticles. A schematic of the structure is shown in figure 10(*a*). A thin film of TiO_2 was deposited onto a quartz substrate. Al nanoparticles were then deposited onto the TiO_2 surface using nanosphere lithography, hence forming an hexagonal array (see the inset in figure 10(*a*)). The photocatalytic activity was evaluated using methylene blue as a test molecule. When the structure is illuminated using UV light, the Al NPs enhance the excitation field seen by the TiO_2 film. The acceleration of the photocatalytic degradation reaction when Al nanoparticles are added is evidenced in figure 10(*b*), where the methylene concentration was measured by absorption spectroscopy during the reaction. A maximum increase of the reaction rate by a factor of ∼14 times was observed for a NP size of 34 nm.

4.5. Structural colours

Metal nanoparticles have been used for ages to create coloured materials. The Roman cup known as the Lycurgus cup, as well as some stained glass windows from medieval churches, were both made by incorporating metal nanoparticles inside the glass. The visible colours are then directly defined by the wavelengths scattered by the metal NPs. If the use of noble metals is appropriate for such finely crafted objects, their price may become an issue when moving to mass-production of objects—for instance the 'plasmonic colour printing' as proposed by Kumar and co-workers [84]. Recently, Clausen *et al* [85] used a plasmonic metasurface made of coupled Al nanodisks and nanoholes to create structural colours in plastic. The plasmonic metasurface was created by using hot embossing from a master mould made by e-beam lithography. A transparent layer finally protects the structure from contamination and scratches. The authors observe structural colours that are relatively angle-independent, due to the specific optical properties of

the hybrid disk/hole plasmonic modes. Their approach is compatible with mass-production as the master mould can be reused and because Al is an inexpensive material.

An even more striking colour reproduction was reported by Tan *et al* [83]. Their colour palette is defined by plasmonic pixels made of Al nanodisks atop dielectric nanopillars made of photoresist, with varying diameters and spacing. The structure is supported by a silicon substrate also covered with Al acting as a 'white' backreflector. To illustrate the quality of the plasmonic colour palette, Tan *et al* have reproduced Claude Monet's painting *Impression, soleil levant* (see figure 11, panel (*a*)) as a $300 \times 300\ \mu m^2$ 'plasmonic painting'. On panel (*b*) is the experimentally reproduced painting using the basic palette, where colours are defined by varying only the nanoparticle sizes. The limited palette is unable to reproduce the colour variations from Monet's painting. In striking contrast, with a dual variation of the size and spacing of the Al nanoparticles, Tan *et al* obtained a vibrant reproduction of the painting, as shown in panel (*c*) (see also the zoom in panel (*d*)). A SEM image of the plasmonic pixels is shown in panel (*e*): the colours seen in figure 11(*c*) are structural colours created by these nanostructures. Such realistic colour reproduction is not limited to fine arts related applications, but also concerns applications like security tagging or information storage. Aluminium plasmonic pixels were also made by Olson *et al* [86], using a periodic pattern of Al nanorods. This design creates bright and tunable colour pixels which are compatible with current display technologies.

4.6. Data storage

As a last reported application of aluminium nanostructures, let us mention heat-assisted magnetic recording. This technique allows high storage densities and is based on a focused laser beam to define the recording zone. The laser locally heats the magnetic material beyond its Curie temperature, lowering its magnetic coercivity and hence allowing recording. As the storage density is directly related to the size of the illuminated zone, various kinds of near-field transducers have been proposed, including the use of surface plasmons [87]. Miao, Stoddart and Hsiang have recently proposed near-field transducers made of aluminium [88]. According to their simulations, Al bow-tie antennas can compete with their noble metal counterparts for heat-assisted magnetic recording, while being more cost-effective and protected from corrosion by the native alumina layer.

5. Conclusion

We have presented here a review of basic and applied work on aluminium plasmonics. We have discussed how the relatively high plasma frequency of bulk aluminium ultimately leads to the possibility of extending plasmonics from the visible into the UV, thereby opening interesting avenues in the realms of chemical and biochemical, catalysis and optoelectronics. We stress that while our review has not been exhaustive, we hope to have provided the reader with a good idea of the exciting results and possibilities that are coming out of this field of study. Finally, we underline that aluminium is not the only viable alternative to gold and silver for plasmonics [89]. For instance, both magnesium [90] and indium [91] have been recently proposed as valuable plasmonic materials in the UV range.

Acknowledgments

DG thanks M Kociak, J Martin, J Plain and G Wurtz for fruitful discussions. DG also acknowledges support from the Laboratory of Excellence (Labex) ACTION. This work was performed, in part, at the Center for Nanoscale Materials, a US Department of Energy, Office of Science, Office of Basic Energy Sciences User Facility under Contract No. DE-AC02-06CH11357.

References

[1] Raether H 1988 *Surface Plasmons on Smooth and Rough Surfaces and Gratings* (Berlin: Springer)
[2] Bohren C F and Huffman D R 1983 *Absorption and Scattering of Light by Small Particles* (New York: Wiley)
[3] Novotny L and Hecht B 2012 *Principles of Nano-Optics* 2nd edn (Cambridge: Cambridge University)
[4] Maier S A, Brongersma M L, Kik P G, Meltzer S, Requicha A A G and Atwater H A 2001 *Adv. Mater.* **13** 1501–5
[5] Ray K, Chowdhury M H and Lakowicz J R 2007 *Anal. Chem.* **79** 6480–7
[6] Chan G H, Zhao J, Schatz G C and Van Duyne R P 2008 *J. Phys. Chem.* C **112** 13958–63
[7] Langhammer C, Schwind M and Zorić B K I 2008 *Nano Lett.* **8** 1461–71
[8] Chowdhury M H, Ray K, Gray S K, Pond J and Lakowicz J R 2009 *Anal. Chem.* **81** 1397–403
[9] Taguchi A, Saito Y, Watanabe K, Yijian S and Kawata S 2012 *Appl. Phys. Lett.* **101** 081110
[10] Knight M W, Liu L, Wang Y, Brown L, Mukherjee S, King N S, Everittand H O, Nordlander P and Halas N J 2012 *Nano Lett.* **12** 6000–4
[11] Maidecchi G *et al* 2013 *Acs Nano* **7** 5834–41
[12] Martin J, Proust J, Gérard D and Plain J 2013 *Opt. Mater. Express* **3** 954–9
[13] McMahon J M, Schatz G C and Gray S K 2013 *Phys. Chem. Chem. Phys.* **15** 5415–23
[14] Hylton N P *et al* 2013 *Sci. Rep.* **3** 2874
[15] Diest K, Liberman V, Lennon D M, Welander P B and Rothschild M 2013 *Opt. Express* **21** 28638
[16] Lozano G, Louwers D J, Rodríguez S R, Murai S, Jansen O T, Verschuuren M A and Gómez Rivas J 2013 *Light: Sci. Appl.* **2** e66
[17] Knight M W, King N S, Liu L, Everitt H O, Nordlander P and Halas N J 2014 *ACS Nano* **8** 834–40
[18] Rodriguez M, Furse C, Shumaker-Parry J S and Blair S 2014 *ACS Photon.* **1** 496–506
[19] Bisio F *et al* 2014 *ACS Nano* **8** 9239–47
[20] Martin J, Kociak M, Mahfoud Z, Proust J, Gérard D and Plain J 2014 *Nano Lett.* **14** 5517–23
[21] Ritchie R H 1957 *Phys. Rev.* **106** 874–81
[22] Powell C J and Swan J B 1959 *Phys. Rev.* **115** 869–75
[23] Feuerbacher B P and Steinmann W 1969 *Opt. Commun.* **1** 81–5
[24] Endriz J G and Spicer W E 1971 *Phys. Rev.* B **4** 4144–59
[25] Endriz J G and Spicer W E 1971 *Phys. Rev.* B **4** 4159–84

[26] Pettit R B, Silcox J and Vincent R 1975 *Phys. Rev.* B **11** 3116–23
[27] Batson P E 1982 *Phys. Rev. Lett.* **49** 936–40
[28] Martin J and Plain J 2015 *J. Phys. D: Appl. Phys.* **18** 184002
[29] Rakic A D 1995 *Appl. Opt.* **34** 4755–67
[30] Johnson P B and Christy R W 1972 *Phys. Rev.* B **6** 4370–9
[31] Beversluis M R, Bouhelier A and Novotny L 2003 *Phys. Rev.* B **68** 115433
[32] Ehrenreich H, Philipp H R and Segall B 1963 *Phys. Rev.* **132** 1918–28
[33] Rai A, Park K, Zhou L and Zachariah M R 2006 *Combust. Theory Modelling* **10** 843–59
[34] Liu Z, Steele J M, Srituravanich W, Pikus Y, Sun C and Zhang X 2005 *Nano Lett.* **5** 1726–9
[35] Gryczynski I, Malicka J, Gryczynski Z, Nowaczyk K and Lakowicz J R 2004 *Analyt. Chem.* **76** 4076–81
[36] Foley IV J J, McMahon J M, Schatz G C, Harutyunyan H, Wiederrecht G P and Gray S K 2014 *ACS Photon.* **1** 739–45
[37] Jha S K, Ahmed Z, Agio M, Ekinci Y and Löffler J F 2012 *J. Am. Chem. Soc.* **134** 1966–9
[38] Pakizek T 2011 *J. Phys. Chem.* C **115** 21826–31
[39] Lecarme O, Sun Q, Ueno K and Misawa H 2014 *ACS Photon.* **1** 538–46
[40] Schwind M, Kasemo B and Zorić I 2013 *Nano Lett.* **13** 1743–50
[41] Kauranen M and Zayats A V 2012 *Nat. Photon.* **6** 737–48
[42] Krause D, Teplin C W and Rogers C T 2004 *J. Appl. Phys.* **96** 3626
[43] Castro-Lopez M, Brinks D, Sapienza R and van Hulst N 2011 *Nano Lett.* **11** 4674–8
[44] Melentiev P N, Konstantinova T V, Afanasiev A E, Kuzin A A, Baturin A S, Tausenev A V, Konyaschenko A V and Balykin V I 2013 *Laser Phys. Lett.* **10** 075901
[45] Schwab P M, Moosmann C, Wissert M D, Schmidt E W G, Ilin K S, Siegel M, Lemmer U and Eisler H J 2013 *Nano Lett.* **13** 1535–40
[46] Melentiev P N, Afanasiev A E, Kuzin A A, Baturin A S and Balykin V I 2013 *Opt. Express* **21** 13896
[47] Geddes C D and Lakowicz J R 2002 *J. Fluoresc.* **12** 121–9
[48] Lakowicz J R 2005 *Analyt. Biochem.* **337** 171–94
[49] Fort E and Gresillon S 2008 *J. Phys. D: Appl. Phys.* **41** 013001
[50] Cao S H, Cai W P, Liu Q and Li Y Q 2012 *Annu. Rev. Anal. Chem.* **5** 317–36
[51] Deng W, Xie F, Baltar H T M C M and Goldys E M 2013 *Phys. Chem. Chem. Phys.* **15** 15695–708
[52] Badugu R, Descrovi E and Lakowicz J R 2014 *Analyt. Biochem.* **445** 1–1
[53] Rigneault H, Capoulade J, Dintinger J, Wenger J, Bonod N, Popov E, Ebbesen T W and Lenne P F 2005 *Phys. Rev. Lett.* **95** 4
[54] Gérard D, Wenger J, Bonod N, Popov E, Rigneault H, Mahdavi F, Blair S, Dintinger J and Ebbesen T W 2008 *Phys. Rev.* B **77** 045413
[55] Lu G, Li W, Zhang T, Yue S, Liu J, Hou L, Li Z and Gong Q 2012 *Acs Nano* **6** 1438–48
[56] Mahdavi F and Blair S 2010 *Plasmonics* **5** 169–74
[57] Jiao X and Blair S 2012 *Opt. Express* **20** 29909–22
[58] Ono A, Kikawada M, Akimoto R, Inami W and Kawata Y 2013 *Opt. Express* **21** 17447
[59] Forestiere C, Handin A and Dal Negro L 2014 *Plasmonics* **9** 715–25
[60] Le Ru E V and Etchegoin P G 2009 *Principles of Surface-Enhanced Raman Spectroscopy and Related Plasmonic Effects* (Amsterdam: Elsevier)
[61] Taguchi A, Hayazawa N, Furusawa K, Ishitobi H and Kawata S 2009 *J. Raman Spectrosc.* **40** 1324–30
[62] Dörfer T, Schmitt M and Popp J 2007 *J. Raman Spectrosc.* **38** 1379–82
[63] Mogensen K B, Gühlke M , Kneipp J, Kadkhodazadeh S, Wagner J B, Espina Palanco M, Kneipp H and Kneipp K 2014 *Chem. Commun.* **50** 3744–6
[64] Okamoto K, Niki I, Shvartser A, Narukawa Y, Mukai T and Scherer A 2004 *Nat. Mater.* **3** 601–5
[65] Gao N, Huang K, Li J, Li S, Yang X and Kang J 2012 *Sci. Rep.* **2** 816
[66] Zhang Q, Li G, Liu X, Qian F, Li Y, Sum T C, Lieber C M and Xiong Q 2014 *Nat. Commun.* **5** 5953
[67] Oulton R F, Sorger V J, Zentgraf T, Ma R M, Gladden C, Dai L, Bartal G and Zhang X 2009 *Nature* **461** 629–32
[68] Lawrie B, Kim K W, Norton D and Haglund R 2012 *Nano Lett.* **12** 6152–7
[69] Wu K, Lu Y, He H, Huang J, Zhao B and Ye Z 2011 *J. Appl. Phys.* **110** 023510
[70] Villesen T F, Uhrenfeldt C, Johansen B, Lundsgaard Hansen J, Ulriksen H U and Nylandsted Larsen A 2012 *Nanotechnology* **23** 085202
[71] Zheng B Y, Wang Y, Nordlander P and Halas N J 2014 *Adv. Mater.* **26** 6318–23
[72] Atwater H A and Polman A 2010 *Nat. Mater.* **9** 205–13
[73] Goffard J, Gérard D, Miska P, Baudrion A L, Deturche R and Plain J 2013 *Sci. Rep.* **3** 2672
[74] Mupparapu R, Vynck K, Malfanti I, Vignolini S, Burresi M, Scudo P, Fusco R and Wiersma D S 2012 *Opt. Lett.* **37** 368–70
[75] Lozano G, Grzela G, Verschuuren M A, Ramezani M and Gómez Rivas J 2014 *Nanoscale* **6** 9223–9
[76] Linsebigler A L, Lu G and Yates J T 1995 *Chem. Rev.* **95** 735–58
[77] Herrmann J M 1999 *Catal. Today* **53** 115–29
[78] Dhakshinamoorthy A, Navalon S, Corma A and Garcia H 2012 *Energy Environ. Sci.* **5** 9217–33
[79] Hanaor D A H and Sorrell C C 2014 *Adv. Eng. Mater.* **16** 248–54
[80] Chen J J, Wu J C S, Wu P C and Tsai D P 2012 *J. Phys. Chem.* C **116** 26535–42
[81] Zhang X, Chen Y L, Liu R S and Tsai D P 2013 *Rep. Prog. Phys.* **76** 046401
[82] Honda M, Kumamoto Y, Taguchi A, Saito Y and Kawata S 2014 *Appl. Phys. Lett.* **104** 061108
[83] Tan S J, Zhang L, Zhu D, Goh X M, Wang Y M, Kumar K, Qiu C W and Yang J K W 2014 *Nano Lett.* **14** 4023–9
[84] Kumar K, Duan H, Hegde R S, Koh S C W, Wei J N and Yang J K W 2012 *Nat. Nanotechnol.* **7** 557–61
[85] Clausen J S, Højlund-Nielsen E, Christiansen A B, Yazdi S, Grajower M, Taha H, Levy U, Kristensen A and Mortensen N A 2014 *Nano Lett.* **14** 4499
[86] Olson J, Manjavacas A, Liu L, Chang W S, Foerster B, King N S, Knight M W, Nordlander P, Halas N J and Link S 2014 *Proc. Natl Acad. Sci.*
[87] Challener W A *et al* 2009 *Nat. Photon.* **3** 220–4
[88] Miao L, Stoddart P R and Hsiang T Y 2014 *Nanotechnology* **25** 295202
[89] West P, Ishii S, Naik G, Emani N, Shalaev V and Boltasseva A 2010 *Laser Photon. Rev.* **4** 795–808
[90] Appusamy K, Blair S, Nahata A and Guruswamy S 2014 *Mater. Sci. Eng.* B **181** 77–85
[91] Kumamoto Y, Taguchi A, Honda M, Watanabe K, Saito Y and Kawata S 2014 *ACS Photon.* **1** 598–603